Hydrology and
Earth System
Sciences

Performance of site-specific parameterizations of longwave radiation

Giuseppe Formetta[1]**, Marialaura Bancheri**[2]**, Olaf David**[3]**, and Riccardo Rigon**[2]

[1]Centre for Ecology & Hydrology, Crowmarsh Gifford, Wallingford, UK
[2]Dipartimento di Ingegneria Civile Ambientale e Meccanica, Universita' degli Studi di Trento, Trent, Italy
[3]Dept. of Civil and Environmental Engineering, Colorado State University, Fort Collins, CO, USA

Correspondence to: Giuseppe Formetta (giufor@nerc.ac.uk)

Abstract. In this work 10 algorithms for estimating downwelling longwave atmospheric radiation ($L_\downarrow$) and 1 for upwelling longwave radiation ($L_\uparrow$) are integrated into the JGrass-NewAge modelling system. The algorithms are tested against energy flux measurements available for 24 sites in North America to assess their reliability. These new JGrass-NewAge model components are used (i) to evaluate the performances of simplified models (SMs) of $L_\downarrow$, as presented in literature formulations, and (ii) to determine by automatic calibration the site-specific parameter sets for $L_\downarrow$ in SMs. For locations where calibration is not possible because of a lack of measured data, we perform a multiple regression using on-site variables, i.e. mean annual air temperature, relative humidity, precipitation, and altitude. The regressions are verified through a leave-one-out cross validation, which also gathers information about the possible errors of estimation. Most of the SMs, when executed with parameters derived from the multiple regressions, give enhanced performances compared to the corresponding literature formulation. A sensitivity analysis is carried out for each SM to understand how small variations of a given parameter influence SM performance. Regarding the $L_\downarrow$ simulations, the Brunt (1932) and Idso (1981) SMs, in their literature formulations, provide the best performances in many of the sites. The site-specific parameter calibration improves SM performances compared to their literature formulations. Specifically, the root mean square error (RMSE) is almost halved and the Kling–Gupta efficiency is improved at all sites. Also in this case, Brunt (1932) and Idso (1981) SMs provided the best performances.

The $L_\uparrow$ SM is tested by using three different temperatures (surface soil temperature, air temperature at 2 m elevation, and soil temperature at 4 cm depth) and model performances are then assessed. Results show that the best performances are achieved using the surface soil temperature and the air temperature.

1 Introduction

Longwave radiation is an important component of the radiation balance on earth and it affects many phenomena, such as evapotranspiration, snowmelt (Plüss and Ohmura, 1997), glacier evolution (MacDonell et al., 2013), vegetation dynamics (Rotenberg et al., 1998), plant respiration, and primary productivity (Leigh Jr., 1999). Longwave radiation is usually measured with pyrgeometers, but these are not normally available in basic meteorological stations, even though an increasing number of projects has been developed to fill the gap (Augustine et al., 2000, 2005; Baldocchi et al., 2001). The use of satellite products to estimate longwave solar radiation is increasing (GEWEX, Global Energy and Water cycle Experiment; ISCCP, the International Satellite Cloud Climatology Project), but they have too coarse a spatial resolution for many hydrological uses. Therefore, models have been developed to solve energy transfer equations and compute radiation at the surface (e.g. Key and Schweiger, 1998; Kneizys et al., 1988). These physically based and fully distributed models provide accurate estimates of the radiation components. However, they require input data and model parameters that are not easily available. To overcome this issue, simplified models (SMs), which are based on empirical or physical conceptualizations, have been developed to re-

late longwave radiation to atmospheric proxy data such as air temperature, water vapour deficit, and shortwave radiation. They are widely used and provide clear-sky (e.g. Ångström, 1915; Brunt, 1932; Idso and Jackson, 1969) and all-sky estimations of downwelling ($L_\downarrow$) and upwelling ($L_\uparrow$) longwave radiation (e.g. Brutsaert, 1975; Iziomon et al., 2003a).

SM performances have been assessed in many studies by comparing measured and modelled $L_\downarrow$ at hourly and daily time steps (e.g. Sugita and Brutsaert, 1993a; Iziomon et al., 2003b; Juszak and Pellicciotti, 2013; MacDonell et al., 2013; Schmucki et al., 2014). Hatfield et al. (1983) were among the first to present a comparison of the most used SMs in an evaluation of their accuracy. They tested seven clear-sky algorithms using atmospheric data from different stations in the United States. In order to validate the SMs under different climatic conditions, they performed linear regression analyses on the relationship between simulated and measured $L_\downarrow$ for each algorithm. The results of the study show that the best models were Brunt (1932), Brutsaert (1975) and Idso (1981). Flerchinger et al. (2009) made a similar comparison using more formulations (13) and a wider dataset from North America and China, considering all possible sky conditions. Finally, Carmona et al. (2014) evaluated the performance of six SMs, with both literature and site-specific formulations, under clear-sky conditions for the sub-humid Pampean region of Argentina.

However, none of the above studies have developed a method to systematically estimate site-specific model parameters for location where measurements are not available using basic site characteristics.

This paper introduces the LongWave Radiation Balance package (LWRB) of the JGrass-NewAGE modelling system (Formetta et al., 2014a). LWRB implements 10 formulations for $L_\downarrow$ and 1 for $L_\uparrow$ longwave radiation. The package was systematically tested against measured $L_\downarrow$ and $L_\uparrow$ longwave radiation data from 24 stations across the contiguous USA, chosen from the 65 stations of the AmeriFlux Network. Unlike all previous works, the LWRB component follows the specifications of the Object Modeling System (OMS) framework (David et al., 2013). Therefore, it can use all of the JGrass-NewAGE tools for the automatic calibration algorithms, data management and GIS visualization, and it can be seamlessly integrated into various modelling solutions for the estimation of water budget fluxes (Formetta et al., 2014a). Moreover, differently from other studies, all the tools used in this paper are open-source, well documented, and ready for practical use by other researchers and practitioners.

2 Methodology

The SMs for $L_\uparrow$ (W m^{-2}) and $L_\downarrow$ (W m^{-2}) longwave radiation are based on the Stefan–Boltzmann equation:

$$L_\downarrow = \epsilon_{\text{all-sky}} \cdot \sigma \cdot T_a^4, \tag{1}$$

$$L_\uparrow = \epsilon_s \cdot \sigma \cdot T_s^4, \tag{2}$$

where $\sigma = 5.670 \times 10^{-8}$ (W m^{-2} K^{-4}) is the Stefan–Boltzmann constant, T_a (K) is the air temperature, $\epsilon_{\text{all-sky}}$ (–) is the effective atmospheric emissivity, ϵ_s (–) is the soil emissivity and T_s (K) is the surface soil temperature. To account for the increase in $L_\downarrow$ in cloudy conditions, $\epsilon_{\text{all-sky}}$ (–) is formulated according to Eq. (3):

$$\epsilon_{\text{all-sky}} = \epsilon_{\text{clear}} \cdot \left(1 + a \cdot c^b\right), \tag{3}$$

where c (–) is the cloud cover fraction and a (–) and b (–) are two calibration coefficients. Site-specific values of a and b are presented in Brutsaert (1975) ($a = 0.22$ and $b = 1$), Iziomon et al. (2003a) (a ranges between 0.25 and 0.4 and $b = 2$) and Keding (1989) ($a = 0.183$ and $b = 2.18$). In our modelling system a and b are calibrated to fit measurement data under all sky conditions. The cloud cover fraction, c, can be estimated from solar radiation measurements (Crawford and Duchon, 1999), from visual observations (Alados-Arboledas et al., 1995; Niemelä et al., 2001), and from satellite data (Sugita and Brutsaert, 1993b), or it can be modelled as well. In this study we use the formulation presented in Campbell (1985) and Flerchinger (2000), where c is related to the clearness index s (–), i.e. the ratio between the measured incoming solar radiation, I_m (W m^{-2}), and the theoretical solar radiation computed at the top of the atmosphere, I_{top} (W m^{-2}), according to $c = 1 - s$ (Crawford and Duchon, 1999). This type of formulation needs a shortwave radiation balance model to estimate I_{top} and meteorological stations to measure I_m; also, it cannot estimate c at night. In our application, the fact that the SMs are fully integrated into the JGrass-NewAge system allows us to use the shortwave radiation balance model (Formetta et al., 2013) to compute I_{top}. Night-time values of c are computed with a linear interpolation between its values at the last hour of daylight and the first hour of daylight on consecutive days. The computation of the first and last hours of the day is based on the model proposed in Formetta et al., 2013 that follows the approach proposed in Corripio (2002), Eqs. (4.23)–(4.25). The sunrise occurs at $t = 12 \cdot (1 - \omega/\pi)$ and the sunset will be at $t = 12 \cdot (1 + \omega/\pi)$, where ω is the hour angle, i.e. the angle between the observer meridian and the solar meridian. It is zero at noon and positive before noon. Those equations are based on the assumption that sunrise and sunset occur at the time when the z coordinate of the sun vector equals zero.

The formulation presented in Eq. (3) was proposed by Bolz (1949) applied in other studies (Carmona et al., 2014; Maykut and Church, 1973; Jacobs, 1978; Niemelä et al.,
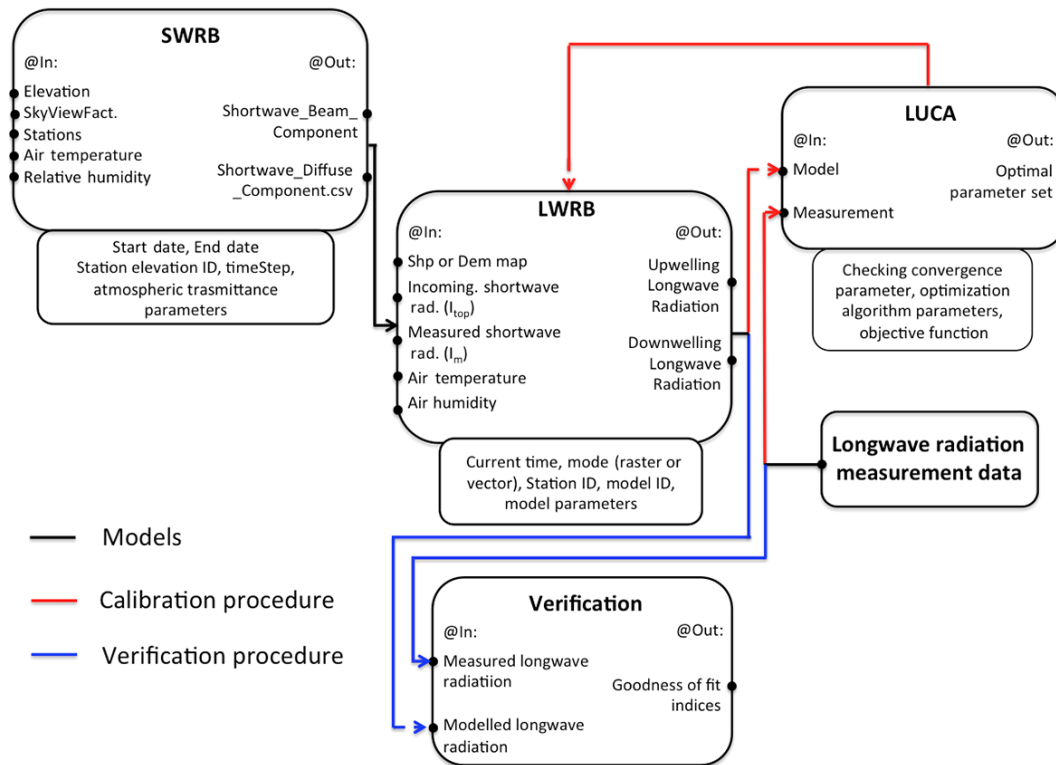
Figure 1. The LWRB component of JGrass-NewAge and the flowchart to model longwave radiation.

2001). Evaluating the effectiveness of different formulations with respect to Eq. (3) is still an open question which is not the object of the current paper. It has been investigated in several studies (i.e. Flerchinger et al., 2009; Juszak and Pellicciotti, 2013, and references therein) and some of them recommended the one proposed by Unsworth and Monteith (1975).

Ten SMs from the literature have been implemented for the computation of ϵ_{clear}. Table 1 specifies assigned component number, component name, defining equation, and reference to the paper from which it is derived. X, Y and Z are the parameters provided in the literature for each model, listed in Table 2.

The models presented in Table 1 were proposed with coefficient values (X, Y, Z) strictly related to the location in which the authors applied the model and where measurements of $L_\downarrow$ radiation were collected. Coefficients reflect climatic, atmospheric and hydrological conditions of the sites, and are reported in Table 2.

The formulation of the $L_\uparrow$ requires the soil emissivity, which usually is a property of the nature of a surface, and the surface soil temperature. Table 3 shows the literature values (Brutsaert, 2005) of the soil emissivity for different surface types: ϵ_s varies from a minimum of 0.95 for bare soils to a maximum of 0.99 for fresh snow.

It is well known that surface soil temperature measurements are only available at a few measurement sites; therefore, under the hypothesis that the difference between soil and air temperatures is not too big, it is possible to simulate $L_\uparrow$ using the air temperature (Park et al., 2008). In our approach three different types of temperature were used to simulate $L_\uparrow$, specifically, surface soil temperature (where available), air temperature at 2 m height, and soil temperature at 4 cm depth.

The LWRB package (see the flowchart in Fig. 1) is part of the JGrass-NewAge system and was first tested in Formetta et al. (2014b). Model inputs depend on the specific SM being implemented and the purpose of the run being performed (calibration, verification, simulation). The inputs are meteorological observations such as air temperature, relative humidity, incoming solar radiation, and sky clearness index. The LWRB is also fed by other JGrass-NewAGE components, such as the shortwave radiation balance (SWRB) (Formetta et al., 2013). To test model performances (i.e. verification), the LWRB can be connected to the system's Verification component; to execute the parameter calibration algorithm (Formetta et al., 2014a), it can be connected to the LUCA (Let Us CAlibrate) component. In turn, all these components can and/or need to be connected to other ones, as the problem under examination may require. Model outputs are $L_\downarrow$ and $L_\uparrow$. These can be provided in single points of specified coordinates or over a whole geographic area, represented as a raster map. For the latter case a digital elevation model (DEM) of the study area is necessary in input.

Table 1. Clear-sky emissivity formulations: T_a is the air temperature (K), w (kg m^{-2}) is precipitable water $= 4650\,(e_0/T_a)$ and e (kPa) is screen-level water-vapour pressure. The models follow the formulations presented and used in Flerchinger (2000). The Angstrom and Brunt models were presented as cited by Niemelä et al. (2001). Konzelmann uses water vapour pressure in Pa, not kPa.

ID	Name	Formulation	Reference
1	Angstrom	$\epsilon_{\text{clear}} = X - Y \times 10^{Ze}$	Ångström (1915)
2	Brunt's	$\epsilon_{\text{clear}} = X + Y \cdot e^{0.5}$	Brunt (1932)
3	Swinbank	$\epsilon_{\text{clear}} = (X \times 10^{-13} \cdot T_a^6)/(\sigma \cdot T_a^4)$	Swinbank (1963)
4	Idso and Jackson	$\epsilon_{\text{clear}} = 1 - X \cdot \exp(-Y \times 10^{-4} \cdot (273 - T_a)^2)$	Idso and Jackson (1969)
5	Brutsaert	$\epsilon_{\text{clear}} = X \cdot (e/T_a)^{1/Z}$	Brutsaert (1975)
6	Idso	$\epsilon_{\text{clear}} = X + Y \times 10^{-4} \cdot e \cdot \exp(1500/T_a)$	Idso (1981)
7	Monteith and Unsworth	$\epsilon_{\text{clear}} = X + Y \cdot \sigma \cdot T_a^4$	Monteith and Unsworth (1990)
8	Konzelmann	$\epsilon_{\text{clear}} = X + Y \cdot (e/T_a)^{1/8}$	Konzelmann et al. (1994)
9	Prata	$\epsilon_{\text{clear}} = [1 - (X + w) \cdot \exp(-(Y + Z \cdot w)^{1/2})]$	Prata (1996)
10	Dilley and O'Brien	$\epsilon_{\text{clear}} = (X + Y \cdot (T_a/273.16)^6 + Z \cdot (w/25)^{1/2})/(\sigma \cdot T_a^4)$	Dilley and O'brien (1998)

Table 2. Model parameter values as presented in their literature formulation.

ID	Name	X	Y	Z
1	Angstrom	0.83	0.18	−0.07
2	Brunt	0.52	0.21	−
3	Swinbank	5.31	−	−
4	Idso and Jackson	0.26	−7.77	−
5	Brutsaert	1.72	7	−
6	Idso	0.70	5.95	−
7	Monteith and Unsworth	−119.00	1.06	−
8	Konzelmann et al.	0.23	0.48	−
9	Prata	1.00	1.20	3.00
10	Dilley and O'brien	59.38	113.70	96.96

Table 3. Soil emissivity for surface types (Brutsaert, 2005).

Nature of surface	Emissivity
Bare soil (mineral)	0.95–0.97
Bare soil (organic)	0.97–0.98
Grassy vegetation	0.97–0.98
Tree vegetation	0.96–0.97
Snow (old)	0.97
Snow (fresh)	0.99

Sections 2.1 and 2.2, respectively, present the calibration and the verification procedure. Moreover, a model sensitivity analysis procedure is presented in Sect. 2.3 and a multi-regression model to relate the optimal parameter set and easily available meteorological data is proposed in Sect. 2.4.

2.1 Calibration of $L_\downarrow$ longwave radiation models

Model calibration estimates the site-specific parameters of $L_\downarrow$ models by tweaking them with a specific algorithm in order to best fit measured data. To this end, we use the LUCA calibration algorithm proposed in Hay et al. (2006), which is a part of the OMS core and is able to optimize parameters of any OMS component. LUCA is a multiple-objective, stepwise, and automated procedure. As with any automatic calibration algorithm, it is based on two elements: a global search algorithm and the objective function(s) to evaluate model performance. In this case, the global search algorithm is the shuffled complex evolution, which has been widely used and described in the literature (e.g. Duan et al., 1993). As the objective function we use the Kling–Gupta efficiency

(KGE, Gupta et al., 2009), which is described below, but LUCA could use other objective functions just as well.

The calibration procedure for $L_\downarrow$ follows these steps.

- The theoretical solar radiation at the top of the atmosphere (I_{top}) is computed using the SWRB (see Fig. 1).

- The clearness index, c, is calculated as the ratio between the measured incoming solar radiation (I_m) and I_{top}.

- Clear-sky and cloud-cover hours are detected by a threshold on the clearness index (equal to 0.6), providing two subsets of measured $L_\downarrow$, which are $L_{\downarrow\text{clear}}$ and $L_{\downarrow\text{cloud}}$. On one side, a threshold of 0.6 to define the clear-sky conditions helps in the sense that it allows us to define time series of measured clear-sky $L_\downarrow$ with comparable length in all the stations, and this is useful for a reliable calibration process. On the other side, it introduces a small error in computing the emissivity in all-sky conditions using Eq. (3). Although the effects of this small error would need further investigations, they could be compensated by the optimization of the parameters a and b that are non-linearly related to the emissivity in all-sky conditions.

- The parameters X, Y, and Z for the models in Table 1 are optimized using the subset $L_{\downarrow\text{clear}}$ and setting $a = 0$ in Eq. (3).

- The parameters a and b for Eq. (3) are optimized using the subset $L_{\downarrow\text{cloud}}$ and using the X, Y, and Z values computed in the previous step.

The calibration procedure provides the optimal set of parameters at a given location for each of the 10 models.

As well as parameter calibration, we carry out a model parameter sensitivity analysis and we provide a linear regression model relating a set of site-specific optimal parameters to mean air temperature, relative humidity, precipitation, and altitude.

2.2 Verification of $L_{\downarrow}$ and $L_{\uparrow}$ longwave radiation models

As presented in previous applications (e.g. Hatfield et al., 1983; Flerchinger et al., 2009), we use the SMs with the original coefficients from the literature (i.e. the parameters of Table 2) and compare the performances of the models against available measurements of $L_{\downarrow}$ and $L_{\uparrow}$ for each site. The goodness of fit is evaluated by using two goodness-of-fit estimators: the Kling–Gupta efficiency (KGE) and the root mean square error (RMSE).

The KGE (Eq. 4) is able to incorporate into one objective function three different statistical measures of the relation between measured (M) and simulated (S) data: (i) the correlation coefficient, r; (ii) the variability error, $a = \sigma_S/\sigma_M$; and (iii) the bias error, $b = \mu_S/\mu_M$. In these definitions μ_S and μ_M are the mean values, while σ_S and σ_M are the standard deviations of measured and simulated time series.

$$\text{KGE} = 1 - \sqrt{(r-1)^2 + (a-1)^2 + (b-1)^2} \qquad (4)$$

The RMSE, on the other hand, is presented in Eq. (5):

$$\text{RMSE} = \sqrt{\frac{1}{N}\sum_{i=1}^{N}(M_i - S_i)^2}, \qquad (5)$$

where M and S represent the measured and simulated time series, respectively, and N is their length.

2.3 Sensitivity analysis of $L_{\downarrow}$ models

For each $L_{\downarrow}$ model we carry out a model parameter sensitivity analysis to investigate the effects and significance of parameters on performance for different model structures (i.e. models with one, two, and three parameters). The analyses are structured according to the following steps:

- we start with the optimal parameter set, computed by the optimization process for the selected model;

- all parameters are kept constant and equal to the optimal parameter set, except for the parameter under analysis;

- 1000 random values of the analysed parameter are picked from a uniform distribution centered on the optimal value with width equal to $\pm 30\%$ of the optimal

value; in this way 1000 model parameter sets were defined and 1000 model runs were performed; and

- 1000 values of KGE are computed by comparing the model outputs with measured time series.

The procedure was repeated for each parameter of each model and for each station of the analysed dataset.

2.4 Regression model for parameters of $L_{\downarrow}$ models

The calibration procedure previously presented to estimate the site-specific parameters for $L_{\downarrow}$ models requires measured downwelling longwave data. Because these measurements are rarely available, we implement a straightforward multivariate linear regression (Chambers, 1992; Wilkinson and Rogers, 1973) to relate the site-specific parameters X, Y and Z to a set of easily available site-specific climatic variables, used as regressors r_i. To perform the regression we use the open-source R software (https://cran.r-project.org) and to select the best regressors we use algorithms known as "best subsets regression", which are available in all common statistical software packages. The regressors we have selected are mean annual air temperature, relative humidity, precipitation, and altitude. The models that we use for the three parameters are presented in Eqs. (6)–(8):

$$X = i_X + \sum_{k=1}^{N}\alpha_k \cdot r_k + \epsilon_X, \qquad (6)$$

$$Y = i_Y + \sum_{k=1}^{N}\beta_k \cdot r_k + \epsilon_Y, \qquad (7)$$

$$Z = i_Z + \sum_{k=1}^{N}\gamma_k \cdot r_k + \epsilon_Z, \qquad (8)$$

where $N = 4$ is the number of regressors (annual mean air temperature, relative humidity, precipitation, and altitude); r_k with $k = 1, \ldots, 4$ are the regressors; i_X, i_Y, and i_Z are the intercepts; α_k, β_k, and γ_k are the coefficients; and ϵ_X, ϵ_Y, and ϵ_Z are the normally distributed errors. Once the regression parameters are determined, the end-user can estimate site-specific X, Y and Z parameter values for any location by simply substituting the values of the regressors in the model formulations.

3 The study area: the AmeriFlux Network

To test and calibrate the LWRB SMs we use 24 meteorological stations of the AmeriFlux Network (http://ameriflux.ornl.gov). AmeriFlux is a network of sites that measure water, energy, and CO_2 ecosystem fluxes in North and South America. The dataset is well known and used in several applications such as Xiao et al. (2010), Barr et al. (2012), and Kelliher et al. (2004). Data used in this study are the Level 2 30 min average data. Complete descriptions and downloads
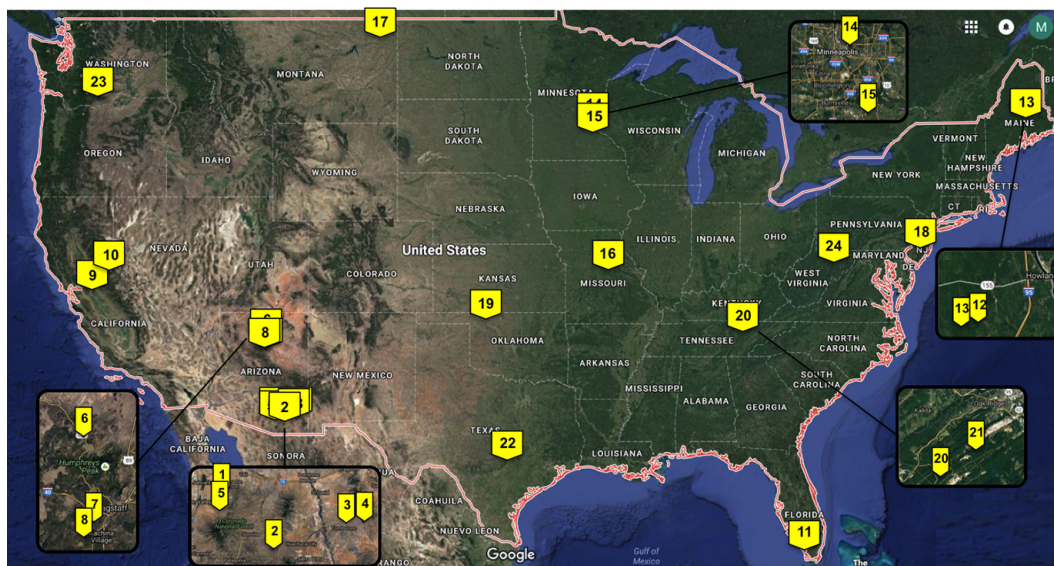
Figure 2. Test site locations in the USA.

are available at the web interface located at http://public.ornl. gov/ameriflux/.

We have chosen 24 sites that are representative of most of the contiguous USA and span a wide climatic range, going from the arid climate of Arizona, where the average air temperature is 16 °C and the annual precipitation is 350 mm, to the equatorial climate of Florida, where the average air temperature is 24 °C and the annual precipitation is 950 mm. Some general and climatic characteristics for each site are summarized in Table 4, while Fig. 2 shows their locations. The 30 min average data have been cumulated to obtain continuous time series of averaged, hourly data for longwave radiation, air and soil temperature, relative humidity, precipitation, and soil water content. Longwave radiation was measured with Eppley pyrgeometers with an uncertainty of $\pm 3 \, \mathrm{W \, m^{-2}}$.

4 Results

4.1 Verification of $L_\downarrow$ models with literature parameters

When implementing the 10 $L_\downarrow$ SMs using the literature parameters, in many cases, they show a strong bias in reproducing measured data. A selection of representative cases is presented in Fig. 3, which shows scatterplots for four SMs in relation to one measurement station. The black points represent the hourly estimates of $L_\downarrow$ provided by literature formulations, while the solid red line represents the line of optimal predictions. Model 1 (Ångström, 1915) shows a tendency to lie below the 1 : 1 line, indicating a negative bias (percent bias of -9.8) and, therefore, an underestimation of $L_\downarrow$. In

contrast, model 9 (Prata, 1996) shows an overestimation of $L_\downarrow$ with a percent bias value of 26.3.
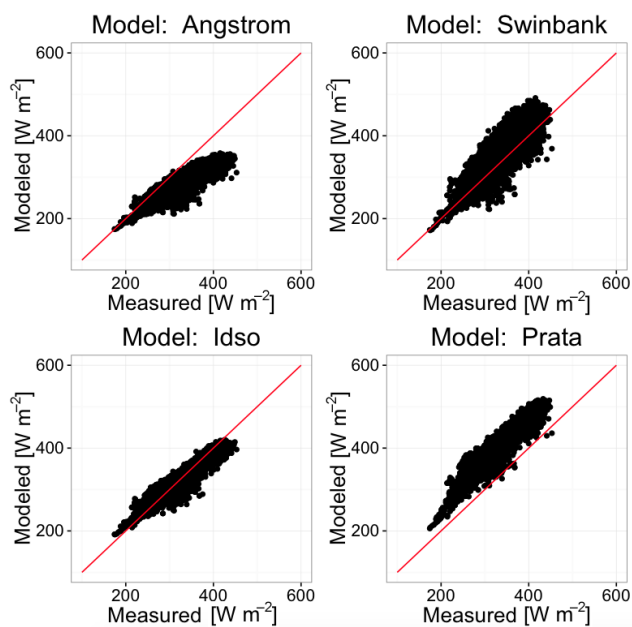
Figure 4 presents the boxplot of KGE (first column) and RMSE (second column) obtained for each model under clear-sky conditions, grouped by classes of latitude and longitude. In general, all the models except Model 8 (Konzelmann et al., 1994) provided values of KGE higher than 0.5 and a RMSE lower than 100 W m^{-2} for all the latitude and longitude classes. Model 8 is the less performing model for many of the stations, likely because the model parameters were estimated for Greenland, where snow and ice play a fundamental role in the energy balance. Its KGE values range between 0.33 and 0.62 on average, while its RMSE values are higher than 100 W m^{-2} except for latitude classes >40° N and longitude classes > −70° W. Model 6 (Idso, 1981) and Model 2 (Brunt, 1932) provide the best results and the lower variability, independently of the latitude and longitude ranges where they are applied. Their average KGE values are between 0.75 and 0.92, while the RMSE has a maximum value of 39 W m^{-2}. Moreover, all the models except 2 and 6 show a high variability of the goodness of fit through the latitude and longitude classes.

4.2 $L_\downarrow$ models with site-specific parameters

The calibration procedure greatly improves the performances of all 10 SMs. Optimized model parameters for each model are reported in the Supplement (Table S1). Figure 5 presents the boxplots of KGE and RMSE values for clear-sky conditions grouped by classes of latitude and longitude. The percentage of KGE improvement ranges from its maximum value of 70 % for Model 8 (which is not, however, representative of the mean behaviour of the SMs) to less than 10 % for

Table 4. Some general and climatic characteristics of the sites used for calibration: elevation is the site elevation above sea level, T is the annual average temperature, and data period refers to the period of available measurements.

Site ID	State	Latitude	Longitude	Elevation (m)	Climate	T (°C)	Data period
1	AZ	31.908	−110.840	991	semi-arid	19	2008–2013
2	AZ	31.591	−110.509	1469	temperate, arid	16	2002–2011
3	AZ	31.744	−110.052	1372	temperate, semi-arid	17	2007–2013
4	AZ	31.737	−109.942	1531	temperate, semi-arid	17	2004–2013
5	AZ	31.821	−110.866	116	subtropical	19	2004–2014
6	AZ	35.445	−111.772	2270	warm temperate	9	2005–2010
7	AZ	35.143	−111.727	2160	warm temperate	9	2005–2010
8	AZ	35.089	−111.762	2180	warm temperate	8	2005–2010
9	CA	37.677	−121.530	323	mild	16	2010–2012
10	CA	38.407	−120.951	129	mediterranean	15	2000–2012
11	FL	25.365	−81.078	0	equatorial savannah	24	2004–2011
12	ME	45.207	−68.725	61	temperate continental	5	1996–2008
13	ME	45.204	−68.740	60	temperate continental	6	1996–2009
14	MN	44.995	−93.186	301	continental	6	2005–2009
15	MN	44.714	−93.090	260	snowy, humid summer	8	2003–2012
16	MO	38.744	−92.200	219	temperate continental	13	2004–2013
17	MT	48.308	−105.102	634	continental	5	2000–2008
18	NJ	39.914	−74.596	30	temperate	12	2005–2012
19	OK	36.427	−99.420	611	cool temperate	15	2009–2012
20	TN	35.931	−84.332	286	temperate continental	15	2005–2011
21	TN	35.959	−84.287	343	temperate	14	1994–2007
22	TX	29.940	−97.990	232	warm temperate	20	2004–2012
23	WA	45.821	−121.952	371	strongly seasonal	9	1998–2013
24	WV	39.063	−79.421	994	temperate	7	2004–2010

Figure 3. Results of the clear-sky simulation for four literature models using data from Howland Forest (Maine).

Model 6, with an average improvement of around 35 %. Even though variations in model performances with longitude and latitude classes still exist when using optimized model parameters, the magnitude of these variations is reduced with respect to the use of literature formulations. The calibration procedure reduces the RMSE values for all the models to below 45 W m^{-2}, even for Model 8, which also in this case had the maximum improvement. Model 6 (Idso, 1981) and Model 2 (Brunt, 1932) provide the best results on average for all the analysed latitude and longitude classes.

Figure 6 presents the boxplots of KGE and RMSE values for each model under all-sky conditions, grouped by latitude and longitude classes. In general, for all-sky conditions we observe a deterioration of KGE and RMSE values with respect to the clear-sky optimized case, with a decrease in KGE values up to a maximum of 25 % on average for Model 10. This may be due to uncertainty incorporated into the formulation of the cloudy-sky correction model (Eq. 3): it seems that sometimes the cloud effects are not accounted for appropriately. This, however, is in line with the findings of Carmona et al. (2014).
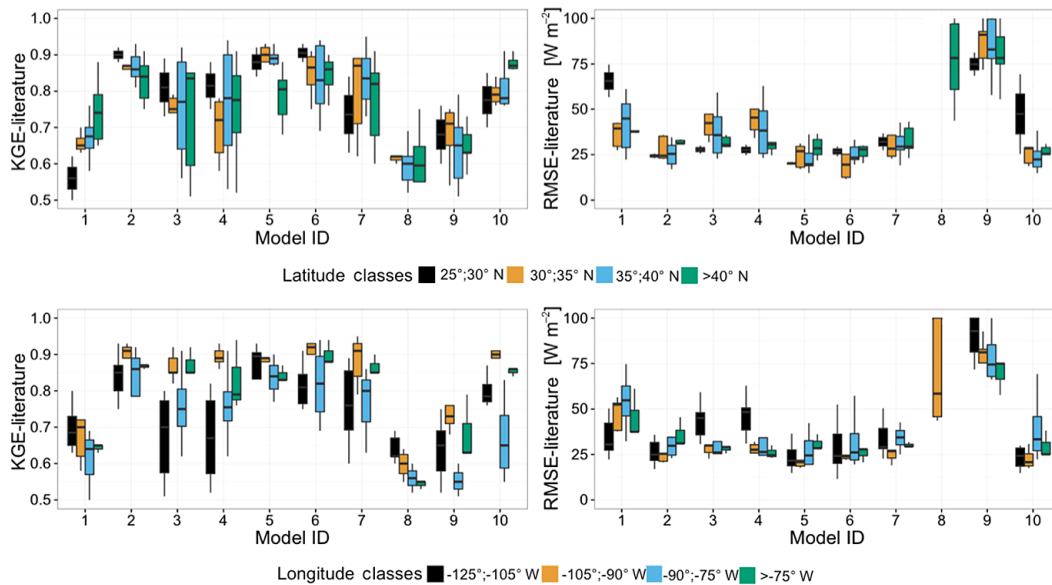
Figure 4. KGE and RMSE values for each clear-sky simulation using literature formulations, grouped by classes of latitude and longitude. Only values of KGE above 0.5 are shown. Only values of RMSE below $100\,\mathrm{W\,m^{-2}}$ are shown.
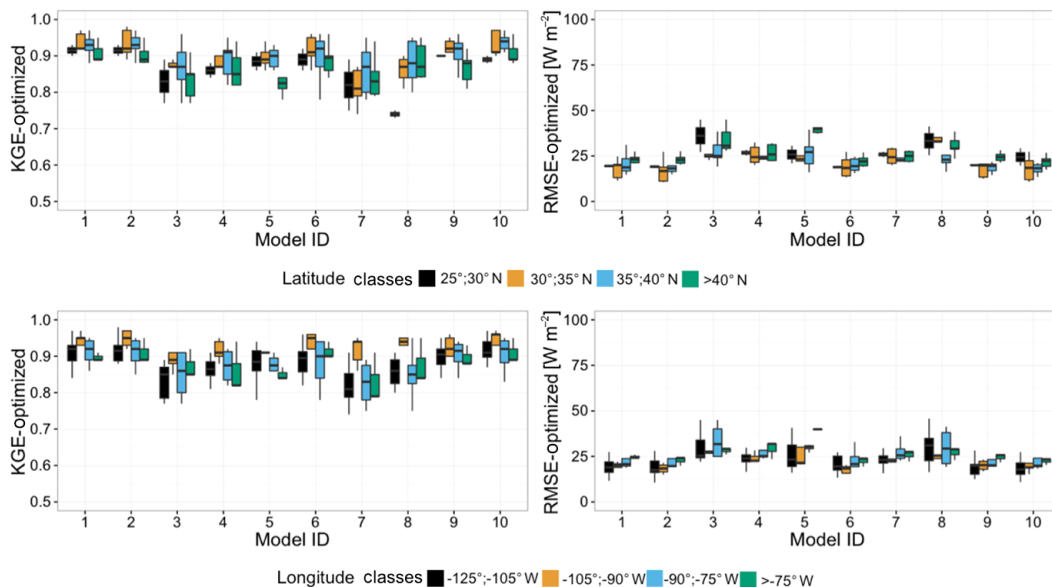

Figure 5. KGE (best is 1) and RMSE (best is 0) values for each optimized formulation in clear-sky conditions, grouped by classes of latitude and longitude. Only values of KGE above 0.5 are shown.

4.3 Sensitivity analysis of $L_\downarrow$ models

The results of the model sensitivity analysis are summarized in Fig. 7a and b for Models 1 to 5 and Models 6 to 10, respectively. Each figure presents three columns, one for each parameter. Considering Model 1 and parameter X: the range of X is subdivided into 10 equal-sized classes and for each class the corresponding KGE values are presented as a boxplot. A smooth blue line passing through the boxplot medi-

ans is added to highlight any possible pattern to parameter sensitivity. A flat line indicates that the model is not sensitive to parameter variation around the optimal value. Results suggest that models with one and two parameters are all sensitive to parameter variation, presenting a peak in KGE in correspondence to their optimal values; this is more evident in models with two parameters. Models with three parameters tend to have at least one insensitive parameter, except for
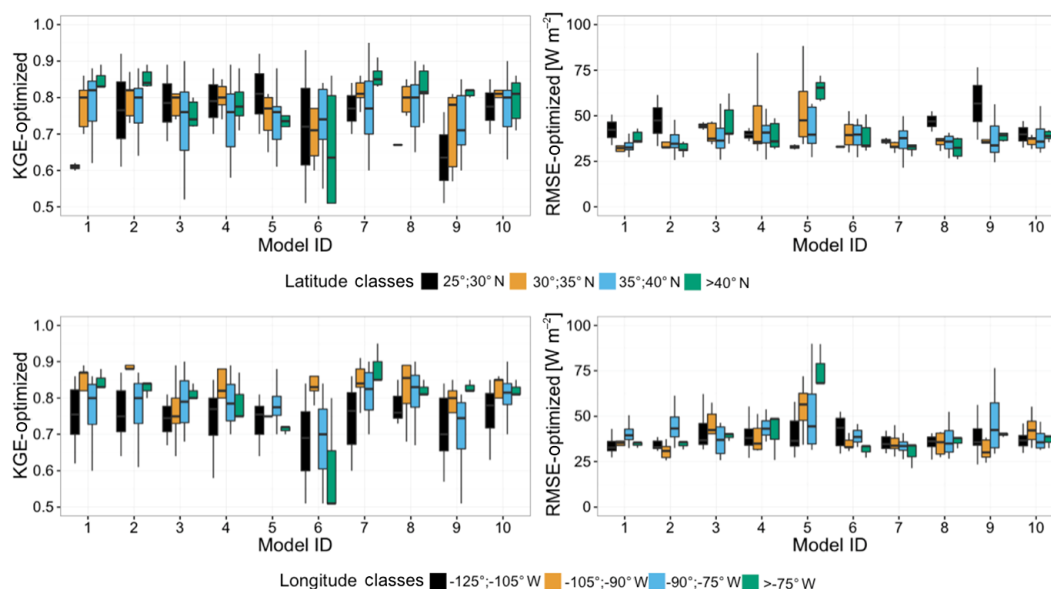
Figure 6. KGE and RMSE values for each model in all-sky conditions with the optimized parameters; results are grouped by classes of latitude and longitude. Only values of KGE above 0.5 are shown.
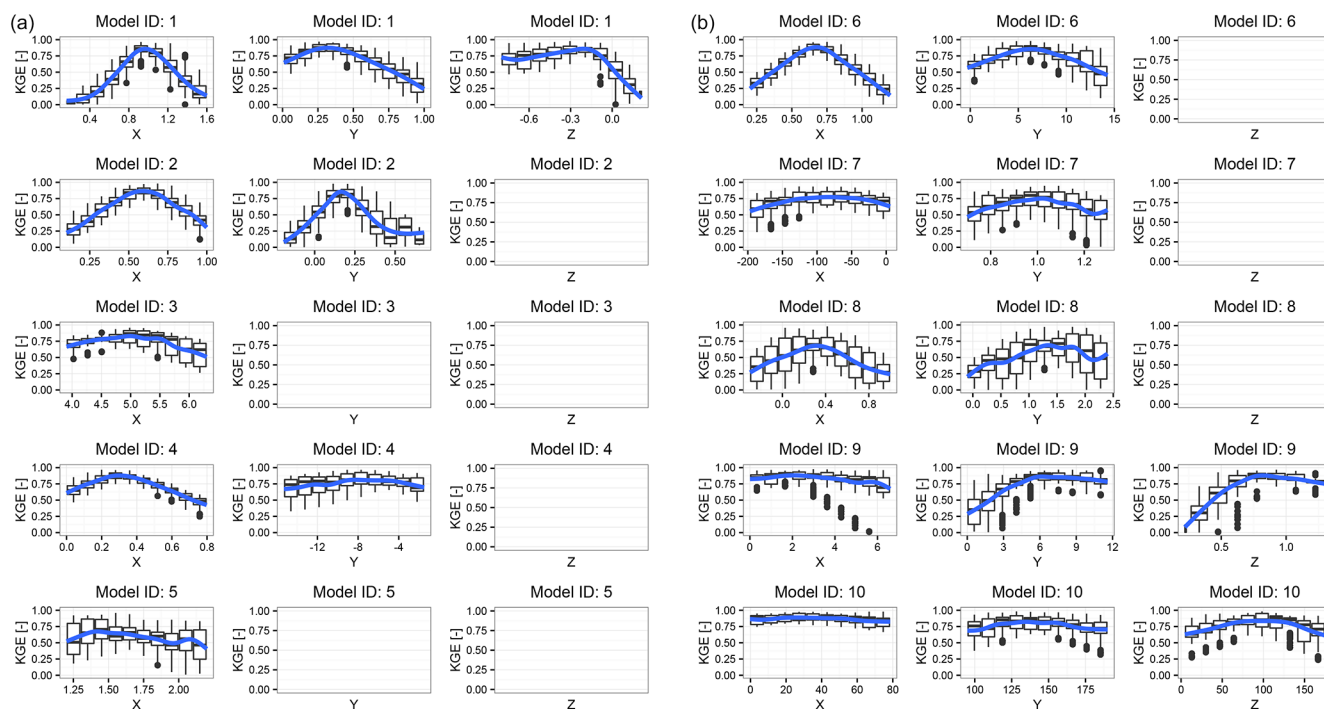

Figure 7. Results of the model parameters' sensitivity analysis. The variation of the model performances due to a variation of one of the optimal parameters and assuming constant the others is presented as a boxplot. The procedure is repeated for each model and the blue line represents the smooth line passing through the boxplot medians.

Model 1, which could reveal a possible overparameterization of the modelling process.

4.4 Regression model for parameters of $L_\downarrow$ models

A multivariate linear regression model was estimated to relate the site-specific parameters X, Y and Z to mean annual

Figure 8. Comparison between model performances obtained with regression and classic parameters: the KGE values shown are those above 0.3 and results are grouped by latitude classes.

air temperature, relative humidity, precipitation, and altitude. The script containing the regression model is available, as specified in the Reproducible Research section below.

The performances of the $L_\downarrow$ models using parameters assessed by linear regression are evaluated through the leave-one-out cross validation (Efron and Efron, 1982). We use 23 stations as training sets for Eqs. (6)–(8) and we perform the model verification on the remaining station. The procedure is repeated for each of the 24 stations.

The cross validation results for all $L_\downarrow$ models and for all stations are presented in Figs. 8 and 9, grouped by classes of latitude and longitude, respectively. They report the KGE comparison between the $L_\downarrow$ models with their original parameters (in black) and with the regression model parameters (in black).

In general, the use of parameters estimated with the regression model gives a good estimation of $L_\downarrow$, with KGE values of up to 0.92. With respect to the classic formulation, model performance with regression parameters improved for all the models independently of the latitude and longitude classes. In particular for Model 8 the KGE improved from 0.26 for the classic formulation to 0.92, on average. Finally, the use of the parameters estimated by the regression model provides a reduction of the model performances' variability for all the models except Models 5 and 8, for longitude classes −125; −105° W and −105; −90° W, respectively.

4.5 Verification of the $L_\uparrow$ model

Figure 10 presents the results of the $L_\uparrow$ simulations obtained using the three different temperatures available at experimental sites: soil surface temperature (skin temperature), air temperature, and soil temperature (measured at 4 cm below the surface). The figure shows the performances of the $L_\uparrow$ model for the three different temperatures used in terms of KGE, grouping all the stations for the whole simulation period according to season. This highlights the different behaviours of the model for periods where the differences in the three temperatures are larger (winter) or negligible (summer). The values of soil emissivity are assigned according the soil surface type, according to Table 4 (Brutsaert, 2005). Although many studies investigated the influence of snow covered area on longwave energy balance (e.g. Plüss and Ohmura, 1997; Sicart et al., 2006), the SMs do not explicitly take it into account. As presented in König-Langlo and Augstein (1994), the effect of snow could be implicitly taken into account by tuning the emissivity parameter.

The best fit between measured and simulated $L_\uparrow$ is obtained with the surface soil temperature, with an all-season average KGE of 0.80. Unfortunately, the soil surface temperature is not an easily available measurement. In fact, it is available only for 8 sites of the 24 in the study area. Very good results are also obtained using the air temperature, where the all-season average KGE is around 0.76. The results using air temperature present much more variance compared to those obtained with the soil surface temperature. However,
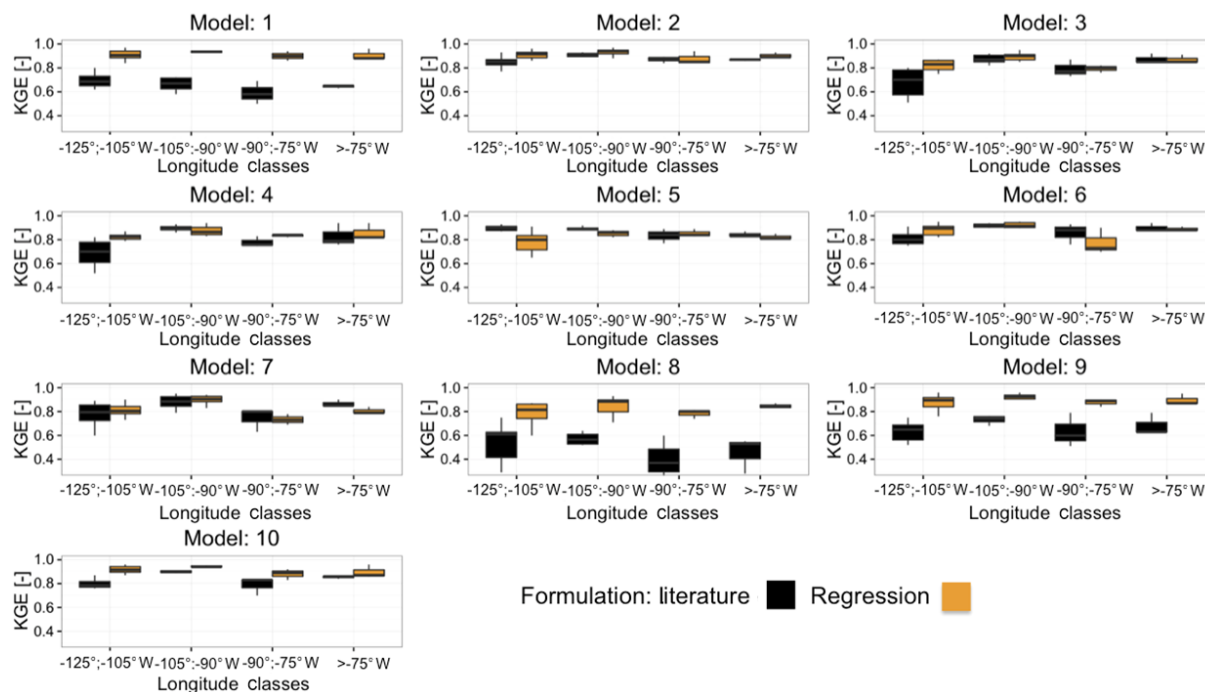
Figure 9. Comparison between model performances obtained with regression and classic parameters: the KGE values shown are those above 0.3 and results are grouped by longitude classes.
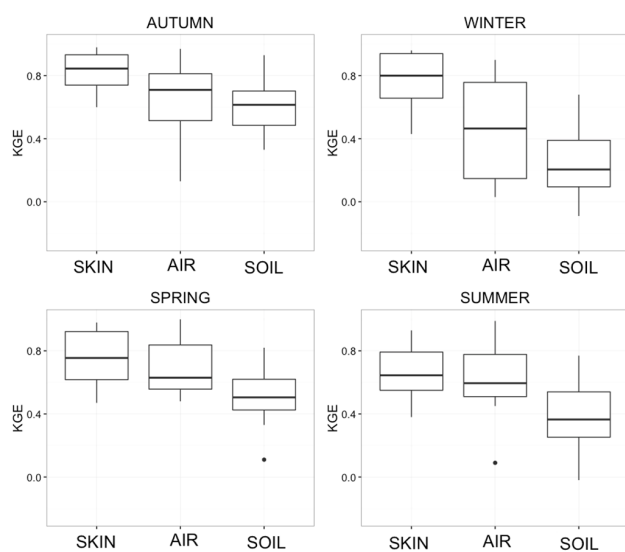

Figure 10. Boxplots of the KGE values obtained by comparing modelled upwelling longwave radiation, computed with different temperatures (soil surface temperature – SKIN, air temperature – AIR, and soil temperature – SOIL), against measured data. Results are grouped by seasons.

air temperature (at 2 m height) is a readily available measure; in fact, it is available for all 24 sites.

The use soil temperature at 4 cm depth provides the least accurate results for our simulations, with an all-season aver-

age KGE of 0.46. In particular, the use of soil temperature at 4 cm depth during the winter is not able to capture the dynamics of $L_\uparrow$. It does, however, show a better fit during the other seasons. This could be because during the winter there is a substantial difference between the soil and skin temperatures, as also suggested in Park et al. (2008).

5 Conclusions

This paper presents the LWRB package, a new modelling component integrated into the JGrass-NewAge system to model upwelling and downwelling longwave radiation. It includes 10 parameterizations for the computation of $L_\downarrow$ longwave radiation and 1 for $L_\uparrow$. The package uses all the features offered by the JGrass-NewAge system, such as algorithms to estimate model parameters and tools for managing and visualizing data in GIS.

The LWRB is tested against measured $L_\downarrow$ and $L_\uparrow$ data from 24 AmeriFlux test sites located all over the contiguous USA. The application for $L_\downarrow$ longwave radiation involves model parameter calibration, model performance assessment, and parameter sensitivity analysis. Furthermore, we provide a regression model that estimates optimal parameter sets on the basis of local climatic variables, such as mean annual air temperature, relative humidity, and precipitation. The application for $L_\uparrow$ longwave radiation includes the evaluation of model performance using three different temperatures.

The main achievements of this work include (i) a broad assessment of the classic $L_\downarrow$ longwave radiation parameterizations, which clearly shows that the Idso (1981) and Brunt (1932) models are the more robust and reliable for all the test sites, confirming previous results (Carmona et al., 2014); (ii) a site-specific assessment of the $L_\downarrow$ longwave radiation model parameters for 24 AmeriFlux sites that improved the performances of all the models; (iii) the set-up of a regression model that provides an estimate of optimal parameter sets on the basis of climatic data; and (iv) an assessment of $L_\uparrow$ model performances for different temperatures (skin temperature, air temperature, and soil temperature at 4 cm below the surface), which shows that the skin and the air temperature are better proxies for the $L_\uparrow$ longwave radiation. Regarding longwave downwelling radiation, the Brunt (1932) model is able to provide on average the best performances with the regression model parameters independently of the latitude and longitude classes. For the Idso (1981) model the formulation with a regression parameter provided lower performances with respect to the literature formulation for latitudes between 25 and 30° N.

The integration of the package into JGrass-NewAge will allow users to build complex modelling solutions for various hydrological scopes. In fact, future work will include the link of the LWRB package to the existing components of JGrass-NewAge to investigate $L_\downarrow$ and $L_\uparrow$ effects on evapotranspiration, snow melting, and glacier evolution. Finally, the methodology proposed in this paper provides the basis for further developments such as the possibility of (i) investigating the effect of different all-sky emissivity formulations and quantifying the influence of the clearness index threshold, (ii) verifying the usefulness of the regression models for climates outside the contiguous USA, and (iii) analysing in a systematic way the uncertainty due to the quality of meteorological input data on the longwave radiation balance in scarce instrumented areas.

6　Data availability

The LWRB package has been implemented according to the object-oriented paradigm, making it flexible and expendable for future improvements and maintenance. Thanks to the Gradle Build tool, an open-source automation system, and Travis CI, a continuous integration service used to build and test software projects, code is tagged for any release and our workflow is traceable. For the present paper we used code version v.0.9. Versions till 0.94 are also available in the repository. Researchers interested in replicating or extending our results are invited to download our codes at https://github.com/geoframecomponents/LongWaveRadiationBalance.

Instructions for using the code can be found at http://geoframe.blogspot.co.uk/2016/04/lwrb-component-latest-documentation.html.

Regression of parameters was performed in R and is available at https://github.com/GEOframeOMSProjects/OMS_Project_LWRB/blob/master/docs/Regression.R.

The Supplement related to this article is available online at doi:10.5194/hess-20-4641-2016-supplement.

References

Alados-Arboledas, L., Vida, J., and Olmo, F.: The estimation of thermal atmospheric radiation under cloudy conditions, Int. J. Climatol., 15, 107–116, 1995.

Ångström, A. K.: A study of the radiation of the atmosphere: based upon observations of the nocturnal radiation during expeditions to Algeria and to California, vol. 65, Smithsonian Institution, 1915.

Augustine, J. A., DeLuisi, J. J., and Long, C. N.: SURFRAD-A national surface radiation budget network for atmospheric research, B. Am. Meteorol. Soc., 81, 2341–2357, 2000.

Augustine, J. A., Hodges, G. B., Cornwall, C. R., Michalsky, J. J., and Medina, C. I.: An update on SURFRAD-The GCOS Surface Radiation budget network for the continental United States, J. Atmos. Ocean. Tech., 22, 1460–1472, 2005.

Baldocchi, D., Falge, E., Gu, L., Olson, R., Hollinger, D., Running, S., Anthoni, P., Bernhofer, C., Davis, K., Evans, R., Fuentes, J., Goldstein, A., Katul, G., Law, B., Lee, X., Malhi, Y., Meyers, T., Munger, W., Oechel, W., Paw, K., Pilegaard, K., Schmid, H., Valentini, R., Verma, S., Vesala, T., Wilson, K.,and Wofsy, S.: FLUXNET: A new tool to study the temporal and spatial variability of ecosystem-scale carbon dioxide, water vapor, and energy flux densities, B. Am. Meteorol. Soc., 82, 2415–2434, 2001.

Barr, J. G., Engel, V., Smith, T. J., and Fuentes, J. D.: Hurricane disturbance and recovery of energy balance, CO_2 fluxes and canopy structure in a mangrove forest of the Florida Everglades, Agr. Forest Meteorol., 153, 54–66, 2012.

Bolz, H.: Die Abhängigkeit der infraroten Gegenstrahlung von der Bewölkung, Z. Meteorol, 3, 201–203, 1949.

Brunt, D.: Notes on radiation in the atmosphere. I, Q. J. Roy. Meteorol. Soc., 58, 389–420, 1932.

Brutsaert, W.: On a derivable formula for long-wave radiation from clear skies, Water Resour. Res., 11, 742–744, 1975.

Brutsaert, W.: Hydrology: an introduction, vol. 61, Wiley Online Library, 2005.

Campbell, G. S.: Soil physics with BASIC: transport models for soil-plant systems, vol. 14, Elsevier Science B.V., Amsterdam, the Netherlands, 1985.

Carmona, F., Rivas, R., and Caselles, V.: Estimation of daytime downward longwave radiation under clear and cloudy skies conditions over a sub-humid region, Theor. Appl. Climatol., 115, 281–295, 2014.

Chambers, J. M.: Linear Models, in: Statistical Models in S, edited by: Chambers, J. M. and Hastie, T. J., Wadsworth & Brooks/Cole, Pacific Grove, California, 1992.

Corripio, J. G.: Modelling the energy balance of high altitude glacierised basins in the Central Andes, PhD thesis, University of Edinburgh, Edinburgh, 2002.

Crawford, T. M. and Duchon, C. E.: An improved parameterization for estimating effective atmospheric emissivity for use in calculating daytime downwelling longwave radiation, J. Appl. Meteorol., 38, 474–480, 1999.

David, O., Ascough, J., Lloyd, W., Green, T., Rojas, K., Leavesley, G., and Ahuja, L.: A software engineering perspective on environmental modeling framework design: The Object Modeling System, Environ. Model. Softw., 39, 201–213, 2013.

Dilley, A. and O'brien, D.: Estimating downward clear sky longwave irradiance at the surface from screen temperature and precipitable water, Q. J. Roy. Meteorol. Soc., 124, 1391–1401, 1998.

Duan, Q., Gupta, V. K., and Sorooshian, S.: Shuffled complex evolution approach for effective and efficient global minimization, J. Optimiz. Theory Appl., 76, 501–521, 1993.

Efron, B. and Efron, B.: The jackknife, the bootstrap and other resampling plans, vol. 38, SIAM, Stanford University, Stanford, California, 1982.

Flerchinger, G.: The Simultaneous Heat and Water (SHAW) Model: Technical Documentation, Northwest Watershed Research Center, Tech. rep., Technical Report NWRC 2000-09, USDA Agricultural Research Service, Boise, Idaho, 37 pp., 2000.

Flerchinger, G., Xaio, W., Marks, D., Sauer, T., and Yu, Q.: Comparison of algorithms for incoming atmospheric long-wave radiation, Water Resour. Res., 45, doi:10.1029/2008WR007394, 2009.

Formetta, G., Rigon, R., Chávez, J. L., and David, O.: Modeling shortwave solar radiation using the JGrass-NewAge system, Geosci. Model Dev., 6, 915–928, doi:10.5194/gmd-6-915-2013, 2013.

Formetta, G., Antonello, A., Franceschi, S., David, O., and Rigon, R.: Hydrological modelling with components: A GIS-based open-source framework, Environ. Model. Softw., 55, 190–200, 2014a.

Formetta, G., David, O., and Rigon, R.: Testing site-specific parameterizations of longwave radiation integrated in a GIS-based hydrological model, International Environmental Modelling and Software Society (iEMSs), 7th Intl. Congress on Env. Modelling and Software, San Diego, CA, USA, 2014b.

Gupta, H. V., Kling, H., Yilmaz, K. K., and Martinez, G. F.: Decomposition of the mean squared error and NSE performance criteria: Implications for improving hydrological modelling, J. Hydrol., 377, 80–91, 2009.

Hatfield, J., Reginato, R. J., and Idso, S.: Comparison of long-wave radiation calculation methods over the United States, Water Resour. Res., 19, 285–288, 1983.

Hay, L. E., Leavesley, G. H., Clark, M. P., Markstrom, S. L., Viger, R. J., and Umemoto, M.: Step wise, multiple objective calibration of a hydrologic model for a snowmelt dominated basin, J. Am. Water Resour. Assoc., 42, 877–890, 2006.

Idso, S. B.: A set of equations for full spectrum and 8-to 14-μm and 10.5-to 12.5-μm thermal radiation from cloudless skies, Water Resour. Res., 17, 295–304, 1981.

Idso, S. B. and Jackson, R. D.: Thermal radiation from the atmosphere, J. Geophys. Res., 74, 5397–5403, 1969.

Iziomon, M. G., Mayer, H., and Matzarakis, A.: Downward atmospheric longwave irradiance under clear and cloudy skies: Measurement and parameterization, J. Atmos. Sol.-Terr. Phy., 65, 1107–1116, 2003a.

Iziomon, M. G., Mayer, H., and Matzarakis, A.: Downward atmospheric longwave irradiance under clear and cloudy skies: Measurement and parameterization, J. Atmos. Sol.-Terr. Phy., 65, 1107–1116, 2003b.

Jacobs, J.: Radiation climate of Broughton Island, Energy budget studies in relation to fast-ice breakup processes in Davis Strait, Pap. 26, Inst. of Arctic and Alp. Res., Univ. of Colorado, Boulder, CO, 105–120, 1978.

Juszak, I. and Pellicciotti, F.: A comparison of parameterizations of incoming longwave radiation over melting glaciers: model robustness and seasonal variability, J. Geophys. Res.-Atmos., 118, 3066–3084, 2013.

Keding, I.: Klimatologische Untersuchung ueber die atmosphaerische Gegenstrahlung und Vergleich vom Berechnungsverfahren anhand langjaehriger Messungen im Oberrheintal, Selbstverlag des Deutschen Wetterdienstes, Offenbach am Main, 1989.

Kelliher, F., Ross, D., Law, B., Baldocchi, D., and Rodda, N.: Limitations to carbon mineralization in litter and mineral soil of young and old ponderosa pine forests, Forest Ecol. Manage., 191, 201–213, 2004.

Key, J. R. and Schweiger, A. J.: Tools for atmospheric radiative transfer: Streamer and FluxNet, Comput. Geosci., 24, 443–451, 1998.

Kneizys, F. X., Shettle, E., Abreu, L., Chetwynd, J., and Anderson, G.: Users guide to LOWTRAN 7, Tech. rep., DTIC Document, Air Force Geophysics Lab., Hanscom AFB, MA, 16 August 1988.

König-Langlo, G. and Augstein, E.: Parameterization of the downward long-wave radiation at the Earth's surface in polar regions, Meteorol. Z., 6, 343–347, 1994.

Konzelmann, T., van de Wal, R. S., Greuell, W., Bintanja, R., Henneken, E. A., and Abe-Ouchi, A.: Parameterization of global and longwave incoming radiation for the Greenland Ice Sheet, Global Planet. Change, 9, 143–164, 1994.

Leigh Jr., E. G.: Tropical Forest Ecology: A View from Barro Colorado Island: A View from Barro Colorado Island, Oxford University Press, Oxford, 1999.

MacDonell, S., Nicholson, L., and Kinnard, C.: Parameterisation of incoming longwave radiation over glacier surfaces in the semi-arid Andes of Chile, Theor. Appl. Climatol., 111, 513–528, 2013.

Maykut, G. A. and Church, P. E.: Radiation climate of Barrow Alaska, 1962–66, J. Appl. Meteorol., 12, 620–628, 1973.

Monteith, J. L. and Unsworth, M.: Principles of Environmental Physics, 4th Edn., Butterworth-Heinemann, Academic Press, Elsevier The Boulevard, Oxford, Amsterdam, Waltham, San Diego, 1990.

Niemelä, S., Räisänen, P., and Savijärvi, H.: Comparison of surface radiative flux parameterizations: Part I: Longwave radiation, Atmos. Res., 58, 1–18, 2001.

Park, G.-H., Gao, X., and Sorooshian, S.: Estimation of surface longwave radiation components from ground-based historical net radiation and weather data, J. Geophys. Res.-Atmos., 113, D04207, doi:10.1029/2007JD008903, 2008.

Plüss, C. and Ohmura, A.: Longwave radiation on snow-covered mountainous surfaces, J. Appl. Meteorol., 36, 818–824, 1997.

Prata, A.: A new long-wave formula for estimating downward clear-sky radiation at the surface, Q. J. Roy. Meteorol. Soc., 122, 1127–1151, 1996.

Rotenberg, E., Mamane, Y., and Joseph, J.: Long wave radiation regime in vegetation-parameterisations for climate research, Environ. Model. Softw., 13, 361–371, 1998.

Schmucki, E., Marty, C., Fierz, C., and Lehning, M.: Evaluation of modelled snow depth and snow water equivalent at three contrasting sites in Switzerland using SNOWPACK simulations driven by different meteorological data input, Cold Reg. Sci. Technol., 99, 27–37, 2014.

Sicart, J.-E., Pomeroy, J., Essery, R., and Bewley, D.: Incoming longwave radiation to melting snow: observations, sensitivity and estimation in northern environments, Hydrol. Process., 20, 3697–3708, 2006.

Sugita, M. and Brutsaert, W.: Cloud effect in the estimation of instantaneous downward longwave radiation, Water Resour. Res., 29, 599–605, 1993a.

Sugita, M. and Brutsaert, W.: Comparison of land surface temperatures derived from satellite observations with ground truth during FIFE, Int. J. Remote Sens., 14, 1659–1676, 1993b.

Swinbank, W. C.: Long-wave radiation from clear skies, Q. J. Roy. Meteorol. Soc., 89, 339–348, 1963.

Unsworth, M. H. and Monteith, J.: Long-wave radiation at the ground I. Angular distribution of incoming radiation, Q. J. Roy. Meteorol. Soc., 101, 13–24, 1975.

Wilkinson, G. and Rogers, C.: Symbolic description of factorial models for analysis of variance, Appl. Stat., 22, 392–399, 1973.

Xiao, J., Zhuang, Q., Law, B. E., Chen, J., Baldocchi, D. D., Cook, D. R., Oren, R., Richardson, A. D., Wharton, S., Ma, S., Martin, T. A., Verma, S. B., Suyker, A. E., Scott, R. L., Monson, R. K., Litvak, M., Hollinger, D. Y., Sun, G., Davis, K. J., Bolstad, P. V., Burns, S. P., Curtis, P. S., Drake, B. G., Falk, M., Fischer, M. L., Foster, D. R., Gu, L., Hadley, J. L., Katul, G. G., Matamala, R., McNulty, S., Meyers, T. P., Munger, W. J., Noormets, A., Oechel, W. C., Paw U, K. T., Schmid, H. P., Starr, G., Torn, M. S., and Wofsy, S. C.: A continuous measure of gross primary production for the conterminous United States derived from MODIS and AmeriFlux data, Remote Sens. Environ., 114, 576–591, 2010.